Artificial Neural Network based Control and Grid Integration of Residential Solar Photovoltaic Systems

P Mohammed Ghouse[1], A. Muni sankar[2], T. Devaraju[3]
PG Student[1], Assistant Professor[2], Professor[3],
Department of Electrical and Electronics Engineering,
Sree Vidyanikethan Engineering College, Tirupati, INDIA

Abstract: A residential solar PV array is usually connected to the distributed grid through a single-phase DC-AC inverter. Control of the single-phase PV system should maximize the power output from the PV array while ensuring overall system performance, safety, reliability, and controllability for interface with the electricity grid. The inverter must maintain a stable DC-link voltage in order to assure efficient and reliable MPPT operation, which is a challenging task especially under fast changing weather conditions. For optimal control and grid integration of residential solar PV systems an Artificial Neural Network (ANN) control strategy based on Approximate Dynamic Programming (ADP) is investigated. The combination of network weights and hyperbolic activation functions allows the ADP-ANN to be able to combine the advantages of proportional-integral (PI), PR, and other optimal control strategies together, making the ADP-ANN control more competitive and powerful than other control methods.

Index Terms–Artificial Neural Networks, DC-AC power converters, DC-DC power converters, dynamic programming, maximum power point tracker, optimal control.

1. INTRODUCTION

A grid connected residential solar PV system consists two parts: 1) a PV array that generates electricity from solar irradiation and 2) power electronic converters for energy extraction and grid integration [1-3]. A PV array is built by certain series and parallel connection of many solar cells together [3].To integrate a residential solar PV systems into the grid, a single-phase DC-AC inverter is commonly introduced and a control strategy for the single-phase inverter needs to be applied to guarantee the stability of the whole system. The inverter must maintain a stable DC-link voltage in order to assure efficient and reliable MPPT operation, which is a challenging task especially under fast changing weather conditions. Among all existing technologies, vector control is usually used to control a three-phase solar inverter [4, 5, 6]. However, to applying vector control to a single-phase inverter, an imaginary circuit needs to be created [7], which has caused challenges to ensure high performance of vector control in

residential solar PV applications, including low reliability under variable PV power generation condition and high harmonic distortion. At present, the dominate control strategy for a single-phase inverter is proportional resonant (PR) control [8] based upon hysteresis switching mechanisms. Compared to vector control, it requires a high sampling frequency (e.g., 10s or 100s kHz) and switching frequency (e.g., 10s or 100s kHz), which would cause more energy loss, larger size of heat sink, and more expensive inverter systems. Another requirement for the grid integration is to mitigate current harmonics injected into the grid from the PV system in order to prevent the malfunction of grid-connected sensitive apparatuses. Hence, a PV system needs to be connected to the grid via a low-pass filter. The common filter topologies consist of L, LC, and LCL filters [9-10]. Compared to L and LC filters, the LCL filter has the best current ripple attenuation ability even with small inductance values. Thus, a low switching frequency can be used by an inverter with a LCL filter [11-14]. Recently, fuzzy and ANN control has been used in solar PV applications. In [15, 16], a fuzzy ANN control strategy is developed for MPPT control. In [17, 18, 19], fuzzy ANN control are developed for control of an L-filter based 3-phase solar inverter. However, none of the previous ANN control techniques is developed to achieve optimal control based on ADP. This paper investigates an artificial neural network (ANN) control strategy based on approximate dynamic programming (ADP) for optimal control and grid integration of residential solar PV systems.

2. RESIDENTIAL PHOTOVOLTAIC SYSTEM

2.1 PV arrays

Solar cells are commonly series connected to form a PV panel that can provide a standard DC voltage. PV panels are connected to form an array to produce desired level of voltage and current [3].

2.2 MPPT Controls

Many MPPT techniques have been proposed for energy extraction from a PV array [15,20, 21]. Among them, Incremental Conductance (IC) method is one of the most popular and widely used [2, 20, 21].

2.3 Solar Inverter

The solar inverter converts the DC output from the DC-DC converter to AC in order for the PV array to be integrated into the grid [4]. This is typically a single-phase inverter for residential applications. The inverter is generally controlled to fulfill the following tasks: 1) stabilizing the DC-link voltage, and 2) regulating reactive power.

2.4 Control Unit

The integrated control unit normally includes two sub control units. One sub-control unit manages the MPPT operation of the PV array through controlling the DC-DC converter. The other sub-control unit is responsible for maintaining the stability of the DC-link voltage and the PCC voltage and for integrating of the PV array into the grid with a power quality, which is achieved through controlling the DC-AC inverter.

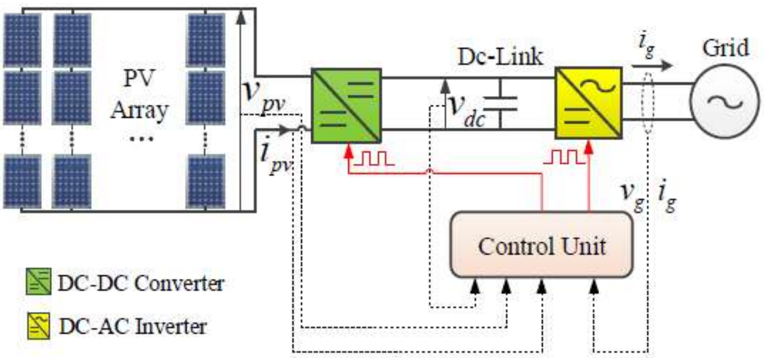

Fig.1. Configuration of grid-connected residential PV system.

3. CONTROL METHODS OF SINGLEPHASE SOLAR INVERTER

3.1 Proportional Resonant Control

PR control is primary control strategy for a single-phase PV inverter [22]. The structure of a common PR control consists of an outer-loop controller and an inner current-loop controller [23]. The outer-loop controller employs the PI controllers to control the DC-link voltage or PCC active power and PCC voltage or reactive power, respectively. Basically, the DC-link voltage or PCC active power controller generates the real component of the reference PCC phasor current while the PCC voltage or reactive power controller generates the imaginary component of the reference PCC phasor current. The real and imaginary components are then multiplied by cos(ωt) and sin(ωt), and their summation is taken as the reference PCC current for the inner current-loop PR controller. The structure of PR controller is shown below

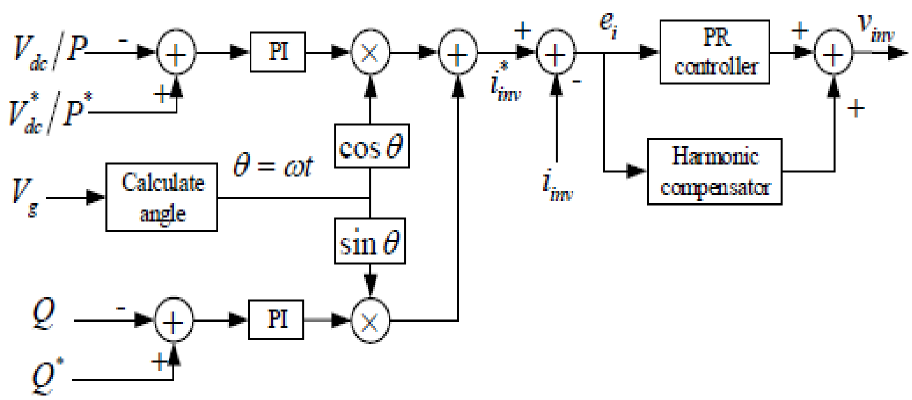

Fig.2 standard PR control configuration

3.2 Conventional Vector Controller

To implement d-q vector control for a single-phase inverter, an imaginary orthogonal circuit of the real circuit is needed. The imaginary circuit has the same circuit components as those shown in the real circuit; the AC voltage and current in the imaginary circuit have the same amplitudes as those of the real circuit but with -90^0 phase shift [24]. Fig. 3 shows both the real and imaginary circuits. The corresponding variables of the imaginary circuit are marked with 'im'. The real and imaginary circuits make up the α-β frame of the single-phase system, which is then transferred into the *d-q* frame through (1).

$$T_{\alpha\beta-dq} = \begin{bmatrix} \cos(\omega t) & \sin(\omega t) \\ -\sin(\omega t) & \cos(\omega t) \end{bmatrix} \tag{1}$$

Three equations in *d-q* frame can be obtained from Fig. 3

$$\begin{bmatrix} v_{c-d} \\ v_{c-q} \end{bmatrix} = R_g \begin{bmatrix} i_{g-d} \\ i_{g-q} \end{bmatrix} + L_g \frac{d}{dt} \begin{bmatrix} i_{g-d} \\ i_{g-q} \end{bmatrix} + \omega L_g \begin{bmatrix} -i_{g-q} \\ i_{g-d} \end{bmatrix} + \begin{bmatrix} v_{g-d} \\ v_{g-q} \end{bmatrix} \tag{2}$$

$$\begin{bmatrix} v_{inv-d} \\ v_{inv-q} \end{bmatrix} = R_g \begin{bmatrix} i_{inv-d} \\ i_{inv-q} \end{bmatrix} + L_{inv} \frac{d}{dt} \begin{bmatrix} i_{inv-d} \\ i_{inv-q} \end{bmatrix} + \omega L_{inv} \begin{bmatrix} -i_{inv-q} \\ i_{inv-d} \end{bmatrix} + \begin{bmatrix} v_{c-d} \\ v_{c-q} \end{bmatrix} \tag{3}$$

$$\begin{bmatrix} i_{inv-d} \\ i_{inv-q} \end{bmatrix} = \begin{bmatrix} i_{g-d} \\ i_{g-q} \end{bmatrix} + C \frac{d}{dt} \begin{bmatrix} v_{c-d} \\ v_{c-q} \end{bmatrix} + C\omega \begin{bmatrix} -v_{c-q} \\ v_{c-d} \end{bmatrix} \tag{4}$$

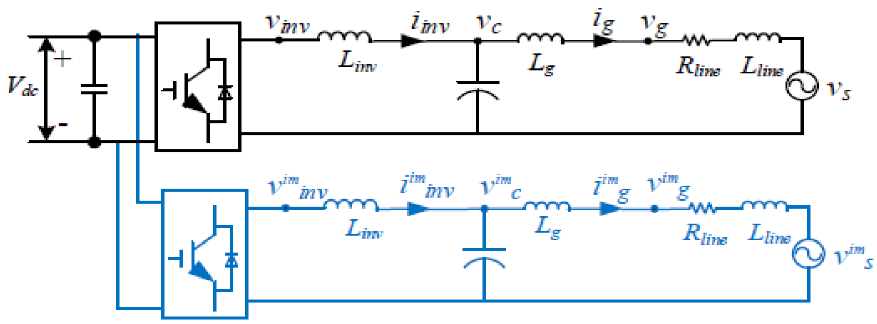
Fig.3 LCL-filter PV inverter: real and imaginary circuits

where R_g represents the resistance in inductor L_g, R_{inv} stands for the resistance in inductor L_{inv}, and ω is the grid-frequency.
Similar to the PR controller, the vector controller usually consists of an outer-loop controller plus an inner-loop current controller as shown in Fig. 5. To develop the inner current controller for an LCL inverter, the conventional strategy is usually to omit the capacitor impact. Hence, (2) to (4) are simplified as (5,6), in which items v'd and v'q are used to design PI controllers for the d- and q-axis loops, and the other terms are treated as compensation items. This approximation would cause a decoupling inaccuracy and instability of the controller. In Fig. 4, $L_{eq}=L_{inv}+Lg$, $i^*_{g\_d}$ and $i^*_{g\_q}$ represent reference *d*- and *q*-axis currents at the PCC.

$$v_{inv-d} = (R_{inv}+R_g)i_{g-d} + (L_{inv}+L_g)\frac{di_{g-d}}{dt} - \omega(L_{inv}+L_g)i_{g-q} + v_{g-d} \quad (5)$$

$$v_{inv-q} = (R_{inv}+R_g)i_{g-q} + (L_{inv}+L_g)\frac{di_{g-q}}{dt} - \omega(L_{inv}+L_g)i_{g-d} + v_{g-q} \quad (6)$$

$$p(t) = \frac{(v_{g-d}.i_{g-d}+v_{g-q}.i_{g-q})}{2} = v_{g-d}.i_{g-d}/2 \quad (7)$$

$$q(t) = \frac{(v_{g-q}.i_{g-d}-v_{g-d}.i_{g-q})}{2} = -v_{g-d}.i_{g-d}/2 \quad (8)$$

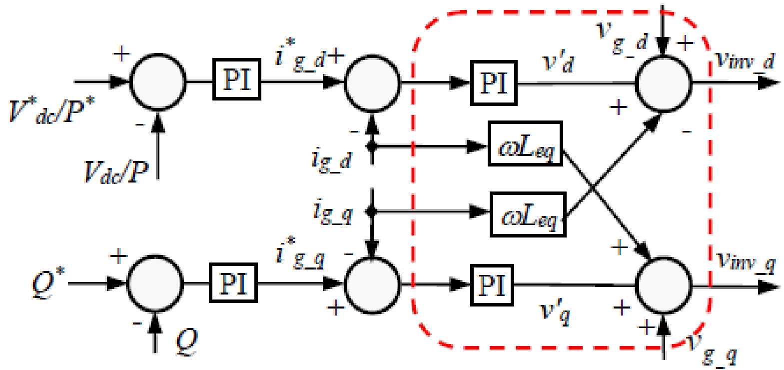

Fig.4 Conventional standard vector control

3.3 Neural Network Current-Loop Vector Control

To address the decoupling inaccuracy issue associated with the conventional vector control, a novel ADP-based ANN current controller is proposed to replace the PI-based current controller as shown by Fig. 5. The ANN portion of the ADP-ANN controller is known as an action network. Firstly, like a conventional controller, we need a dynamic model of the plant, which is eqs. (2) to (4). Secondly, a network structure needs to be specified, which is analogous to specifying a conventional controller structure. Regarding the network structure, the ANN consists of four layers: an input layer, two hidden layers, and an output layer, which is shown in Fig. 5. The input layer contains four inputs. Two of these inputs comprise the vector $\overrightarrow{e_{dq}}(k)$, the error term, and the other two comprise $\overrightarrow{s_{dq}}(k)$, the integral of the error term. Thirdly, the ANN needs training, which is analogous to tuning a conventional controller. These error and integral error terms are defined by

$$\overrightarrow{e_{dq}}(k) = \overrightarrow{i_{dq}}(k) - \overrightarrow{i^*_{dq}}(k), \quad \overrightarrow{s_{dq}}(k) = \int_0^k \overrightarrow{e_{dq}}(k)dt \quad (9)$$

Then, these inputs are divided by their appropriate gains, and hyperbolic tangents are used on them. The outputs of the input layer feed forward to the two hidden layers of six nodes, each node with a hyperbolic tangent function. The number of hidden layers and number of nodes in each hidden layer are determined via trail and errors. Finally, the output layer translates the output of the action network into $\overrightarrow{v^*_{inv-dq}}(k)$. As the ratio of the inverter output voltage $\overrightarrow{v^*_{inv-dq}}$ to the action network output $\overrightarrow{v^*}_{inv-dq}$ is the gain of the pulse-width-modulation (PWM), which is denoted as k_{PWM}, the final control action $\overrightarrow{v^*}_{inv-dq}$ outputted by the inverter is then

$$\overrightarrow{v^*}_{inv-dq}(k) = k_{PWM}\ .A(\overrightarrow{e_{dq}}(k), \overrightarrow{s_{dq}}(k), \omega) \quad (10)$$

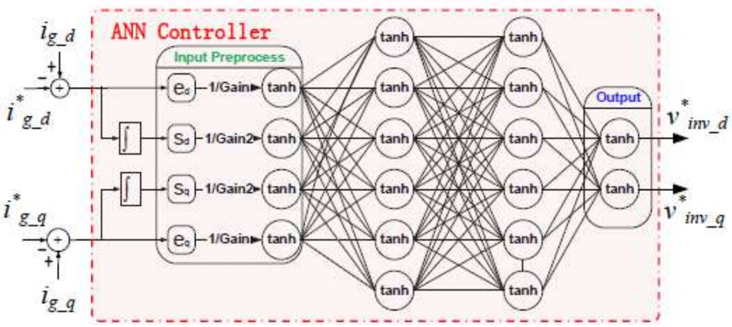

Fig.5 Neural network current loop vector control

3.4 Training ADP-ANN Vector Controller

Training the ADP-ANN controller means tuning the network weights until the ANN learns to control the PV inverter for grid integration adequately based on ADP. This consists of defining a training objective. Firstly, the training objective is to minimize a defined cost function, based on ADP so as to realize ADP-based optimal control [25]. The ADP cost function used in this paper is:

$$C(\overrightarrow{i_{g-dq}}) = \sum_{k=1}^{N}\left(\left[i_{g-d}(k) - i^*_{g-d}\right]^2 + \left[i_{g-q}(k) - i^*_{g-q}\right]^2\right) \quad (11)$$

Hence, the objective is to make the actual d-q current track the d-q reference current as closely as possible.

Secondly, the weights of the action network are tuned to minimize the ADP cost function (9) by using the Levenberg- Marquardt (LM) optimization method [26]. The LM algorithm is a variation of gradient descent which has proven to be one of the most powerful training algorithms for neural networks [27]. For training the network shown in this paper, the gradient of (11) is computed first with respect to the weight vector $\frac{\partial C}{\partial \vec{\omega}}$. In matrix form this is:

$$\frac{\partial C}{\partial \vec{\omega}} = \frac{\partial \sum_{k=1}^{N}(V(k))^2}{\partial \vec{\omega}} = \sum_{k=1}^{n} 2V(k)\frac{\partial V(k)}{\partial \vec{\omega}}\, 2J_p(\vec{\omega}^T)V \tag{12}$$

Where $V(k) = \left[i_{g-d}(k) - i^*_{g-d}\right]^2 + \left[i_{g-q}(k) - i^*_{g-q}\right]^2$ and Vis a vector containing V(1) to V(N) and$J_p(\vec{\omega})$ is a Jacobian matrixdefined for a recurrent neural network by:

$$J_p(\vec{\omega}) = \left[\begin{pmatrix} \frac{\partial V(1)}{\partial \omega_1} & \cdots & \frac{\partial V(1)}{\partial \omega_M} \\ \vdots & \ddots & \vdots \\ \frac{\partial V(N)}{\partial \omega_1} & \cdots & \frac{\partial V(N)}{\partial \omega_M} \end{pmatrix}\right],\ V = \begin{bmatrix} V(1) \\ \vdots \\ VN \end{bmatrix} \tag{13}$$

Using these definitions, the LM weight update is applied as:

$$\Delta\vec{\omega} = -\left[J_p(\vec{\omega}^T)\, J_p(\vec{\omega}) + \mu I\right]^{-1} J_p(\vec{\omega}^T)V \tag{14}$$

$$\vec{\omega}_{update} = \vec{\omega} + \Delta\vec{\omega} \tag{15}$$

Whereµ is a scalar regulation parameter that is dynamically adjusted during the training. As show, the Jacobian matrix $J_p(\vec{\omega})$is the core for training used by the LM method.

4. INTEGRATING MPPT AND ANN CONTROL

4.1 MPPT control:

IC MPPT approach is used to extract the maximum power from a PV array. The IC MPPT controller was initially tuned by considering the PV array and DC-DC converter only under a constant DC-link voltage condition. After the MPPT controller is tuned, the PV array is connected to the grid through the single-phase inverter. However, the integration may cause large oscillation of the DC-link voltage, especially under intermittent solar irradiance conditions. This may affect the MPPT efficiency and potential trip of the PV system. Thus, maintaining the stability of DC-link voltage is critical for connecting the PV system to the grid.

4.2 Artificial Neural Network Control

An ADP-ANN controller must be trained before applying it to the overall PV system. The training was based upon the independent inverter structure shown by Fig.5, in which both the DC-link voltage and grid PCC voltage are considered as constant. The ANN was trained repeatedly to track a variety of reference d-q current trajectories until satisfactory and excellent tracking performance is achieved. Each training experiment starts with randomly generated network weights. Thus, each may converge to different ADP cost. The final network weights are selected from those training experiments having the lowest ADP costs. After the network is well trained, the ANN controller for simulation or experiment case is able to track reference d-q current with minimum errors and in the optimal way according to ADP.

Note: the ANN is trained offline, and no training occurs in the real-time control stage. Besides, although it is impossible for the training current trajectories to cover all current transient conditions, such as startup and power system transient events, the trained ANN controller has strong ability to track a broad reference current trajectory that are not presented in the training data set. In simulation, we have tested various startup and transient cases and the ADP-ANN controller has demonstrated great performance and robustness.

4.3 Integrating MPPT and ANN Controls:

The integration of MPPT and ANN controllers is based on the PV system shown by Fig.6. The MPPT controller is responsible for extracting power from the PV array with the maximum efficiency. Depending on the irradiance levels, the extracted power could go up and down, causing the DC-link voltage to increase and decrease. The stability of the DC-link voltage is maintained through the ANN controller. To achieve this, a PI-based DC-link voltage controller is added before the ANN current tracking controller. According to 7, this is achieved through the control of the PCC d-axis current. As shown by Fig.6, the DC-link voltage controller generates a d-axis current reference to the ANN controller based on the error signal between the measured and reference DC-link voltages. The q-axis current tracking ability of the ANN controller is used for another control purpose. According to 8, this could be either reactive power control or grid voltage support control at the PCC. For reactive power control, a PI-based reactive power controller is added before the ANN current tracking controller. The reactive power controller generates a q-axis current reference to the ANN controller based on the error signal between the measured and reference PCC reactive power. For grid voltage support control at the PCC, a PI-based PCC voltage controller is used to generate a q-axis current reference to the ANN controller based on the error signal between the measured and reference PCC voltages. Certainly, the controller gains of the PCC voltage controller would be different from those of the reactive power controller. The PI gains of the DC-link voltage controller and reactive power or PCC voltage support controller were initially tuned without considering the PV array and MPPT control. Also, the ANN controllers are trained for current tracking purpose only. Thus, detailed performance evaluation of the overall integrated system is needed and important, in which we found that PI gains of the DC-link voltage controller and the reactive power or PCC voltage controller usually need to be re-tuned through trial and error to achieve the best control performance regarding the stability and response speed, particularly if the ANN current controller is replaced by a conventional current controller. The simulink implementation of the MPPT and ANN control algorithms is also shown in Fig.6. Within the MPPT algorithm, $dI_{pv}/dV_{pv}$and$I_{pv}/V_{pv}$are first calculated based onPV array terminal voltage and current. Then, the summation of$\frac{dI_{pv}}{dV_{pv}} + \frac{I_{pv}}{V_{pv}}$is used to determineΔD, the duty cyclecorrection, to update duty ratio for control of the DC-DC converter. Within the ANN control algorithm, the PCC voltage $V_g$is used to determine the angular position ofV_g, which is needed for transformation of the PCC sinusoidal current to its d-q representation and inverse transformation of d-q control voltage to its sinusoidal representation. The outer loop controller produces the reference d-q current based on DC-link voltage and PCC reactive power. The difference between the measured and reference d-q currents is used to produce the error and integral of error terms for the ANN controller. The d-q control voltage generated by the ANN is converted into sinusoidal voltage for control of the DC-AC inverter.

5. SIMULATION RESULTS AND COMPARISON

5.1 Steady state Irradiation:

To evaluate MPPT, DC-link voltage and grid reactive power or grid voltage support controls, an integrated transient simulation system of a residential solar PV system (Fig. 6) is developed by using Sim Power Systems, in which both steady and variable solar irradiance conditions are considered. The PV array has a series-parallel connection. The switching frequency is 9 kHz for the DC-DC converter. For the DC-AC inverter, the switching frequency is 7.2 kHz for the conventional and ADP-ANN vector controllers but 15 kHz for the PR controller. Note: a high switching frequency is necessary for a low total harmonic distortion (THD) using the PR control approach. The sampling time is 0.1ms. For the conventional vector control, a passive damping technique is used to prevent instability problem related to resonance by series connecting a resistor with the LCL-capacitor.

Parameters of PV module:

Parameter	Units
Maximum power	135W
Open circuit voltage	86.8V
Short circuit current	2.02A
Maximum voltage	70.4V
Maximum current	1.93A

Table 1: Parameters of PV module

Parameters of PV Inverter:

Parameter	Units
Grid voltage	230V
Grid frequency	50Hz
DC-link voltage	250V
Grid side inductor	0.03H
Inverter side inductor	0.03H
LCL-filter capacitor	1.0 μ F

Table 2: Parameters of PV inverter

Figure 6 presents a case study of the single-phase solar PV system using PR and ANN and conventional vector control approaches under a steady solar irradiation condition. The transmission line resistance is 0.077Ω and inductance is 1mH. For PR and ANN, the LCL damping resistance R_{pd} is not included. Initially, the controller is turned on to build up a stable DC-link voltage via the DC-AC inverter. Then the PV array is connected to the DC-DC converter having a fixed duty ratio at 0.3sec and MPPT starts to be functional at 0.5sec. During the simulation process, the solar irradiation is initially 700W/m^2 and changes to 500W/m^2 at 1.5sec. Note: initial tracking of MPP is slow between 0.5sec and 1.5sec since the initial duty ratio is far away from a MPP. After a MPP is reached, tracking of MPPs is much faster since only a small adjustment is needed to track a new MPP .Similar MPPT performance can be observed for all the three control approaches. For the ANN and PR controlled PV system, although the damping resistance R_{pd} is not applied, the DC-link voltage is maintained at the reference voltage effectively, and the current injected into the grid has a low harmonic distortion. For the PV system using the conventional controller without the damping resistance, the stability of the system cannot be maintained and the harmonic distortion of the AC system current is much worse than the ANN controlled one. But, if the damping resistance is added, the performance of the conventional standard vector control approach is much more improved. Clearly, more losses will be resulted due to the added resistance. Although the damping resistance is added for the conventional vector control approach, the current harmonic Distortion of the PV system is still slightly worse than the PR and ANN controlled one. A special synchronization control strategy is not implemented. Instead, the converter is connected to the grid directly for the purpose to investigate what differences are between the three control techniques for direct connection of the PV system without a synchronization mechanism.

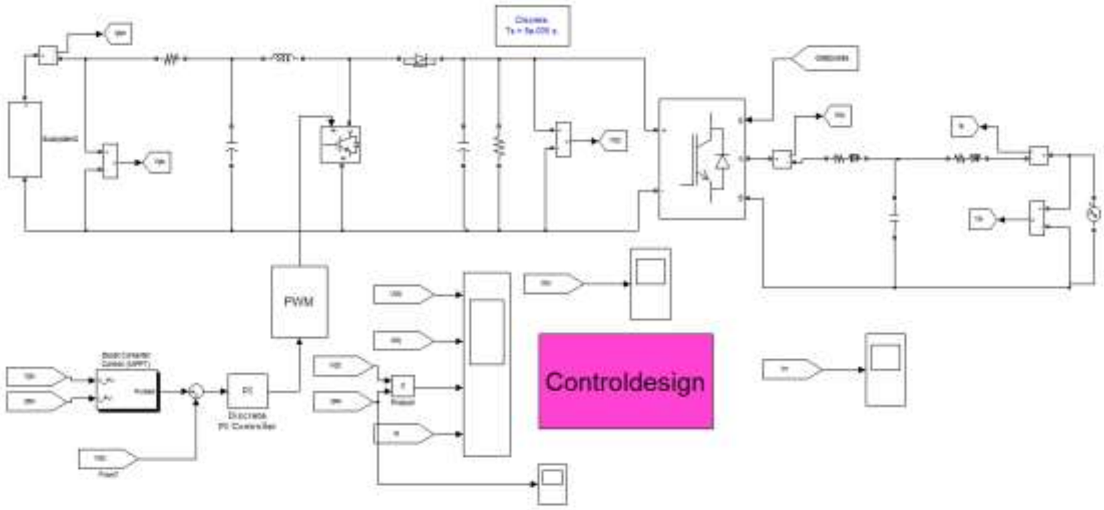

Fig.6 Residential solar photovoltaic systems for MPPT and grid integration

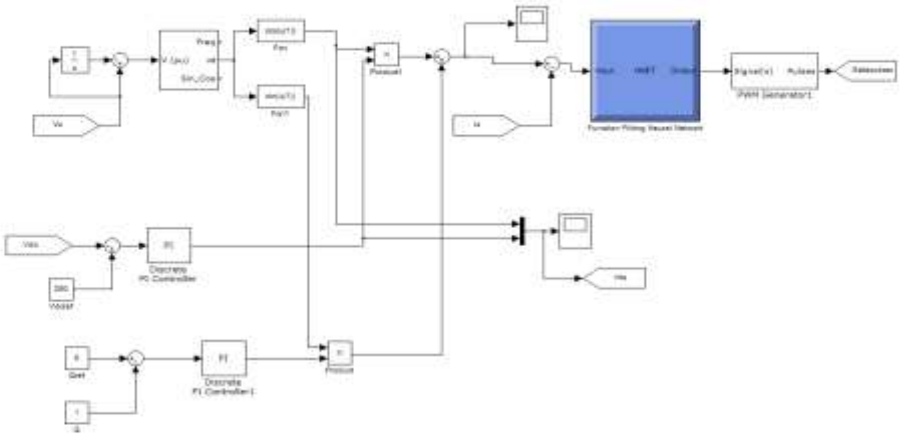

Fig.7 ANN control algorithm

As the ANN controller has a much faster response speed than the PR and conventional vector controllers, the PI gains of the outer control loop can be tuned much larger for the ANN controller than for the PR and conventional vector controllers, which means faster tracking speed of the DC-link or grid voltage while maintaining the stability of the system using the ANN control. Consequently, when initially connecting the solar inverter to the grid even without a synchronization control strategy, the ANN controlled PV system can be quickly connected to the grid with very small oscillation while the PR and conventional vector controlled ones show a high oscillation. Similarly, when there is an increase or decrease of solar radiation causing the DC-link voltage to rise or drop, the ANN controlled one shows much lower overshoot in DC-link voltage than the other two. It is notable that since $i^*_{g\text{-}d}$ is generated from the outer PI loop which controls DC link voltage, an overshoot is always inevitable.

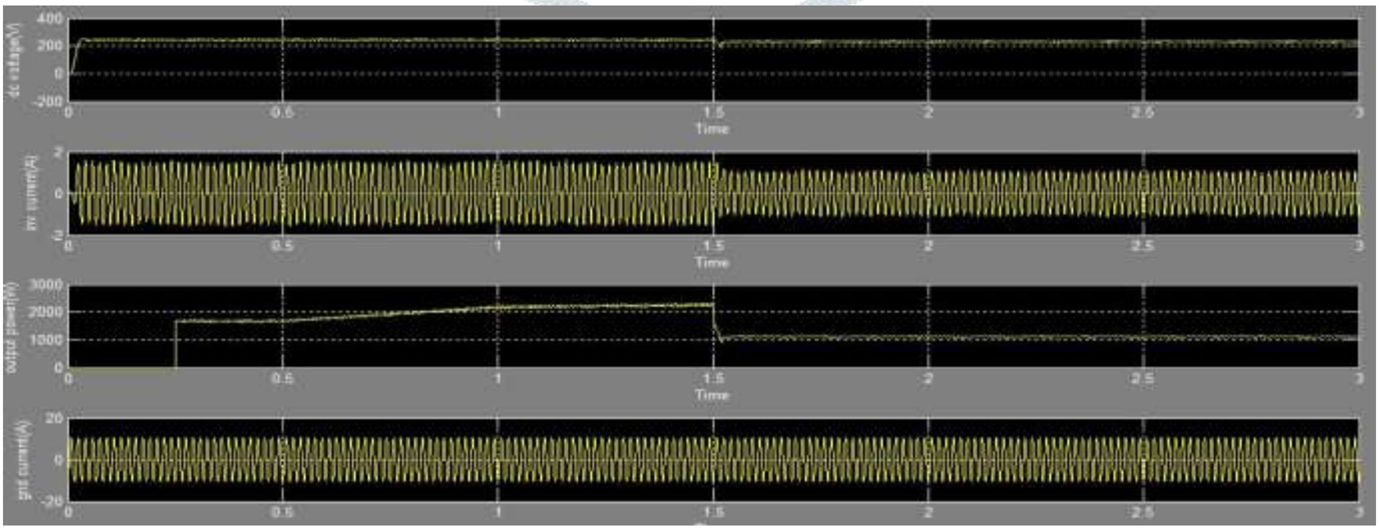

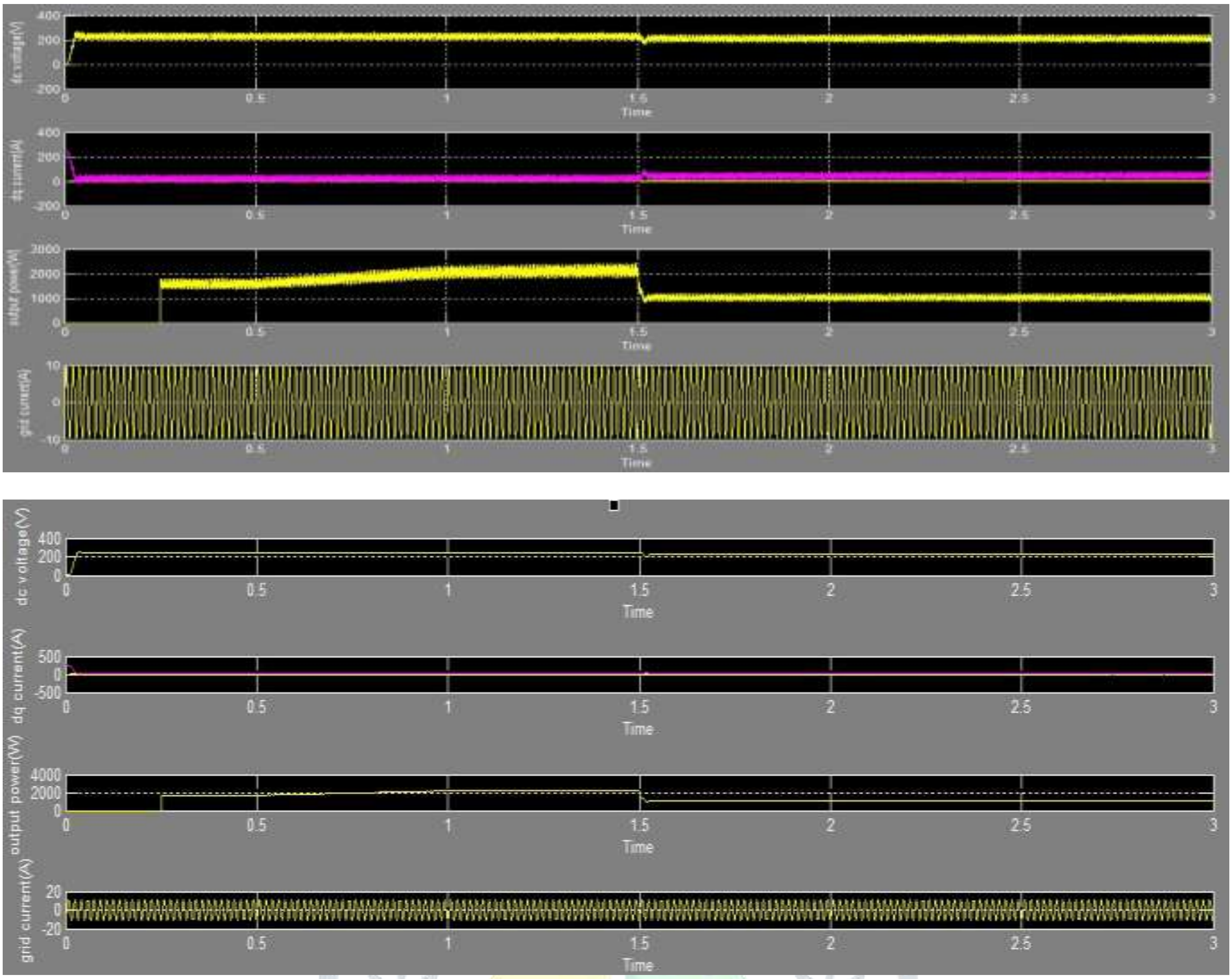

Fig.8 PR, Vector control and ANN control methods for constant irradiation:

5.2 Variable Solar Irradiation

A case study of the solar PV system using PR and ANN and conventional vector control approaches under a variable solar irradiation condition is conducted, which may represent a cloudy weather situation. The per unit solar irradiation relevant to the clear sky(1000W/m^2) I_{rr}. The line resistance and inductance are the same as those used before. Again, for the PR- and ANN-based PV system, the LCL damping resistance R_{pd} is not included. As shown by Fig.9, using the ANN controller, the DC-link voltage oscillates slightly around the reference voltage due to the variable solar irradiation. The MPPT efficiency is not affected, and the PCC current shows a low harmonic distortion. For the solar inverter using the PR and conventional vector control (with the damping resistance) approaches, the DC-link voltage oscillates greatly as the solar irradiation level changes (Fig. 9), which may trigger the DC voltage protection in a practical application.

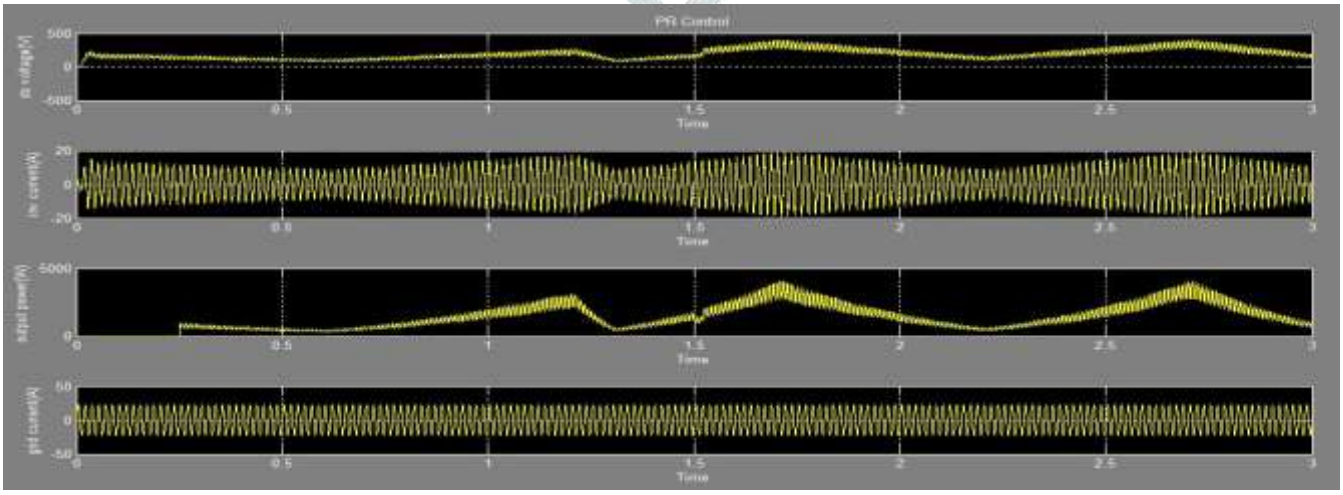

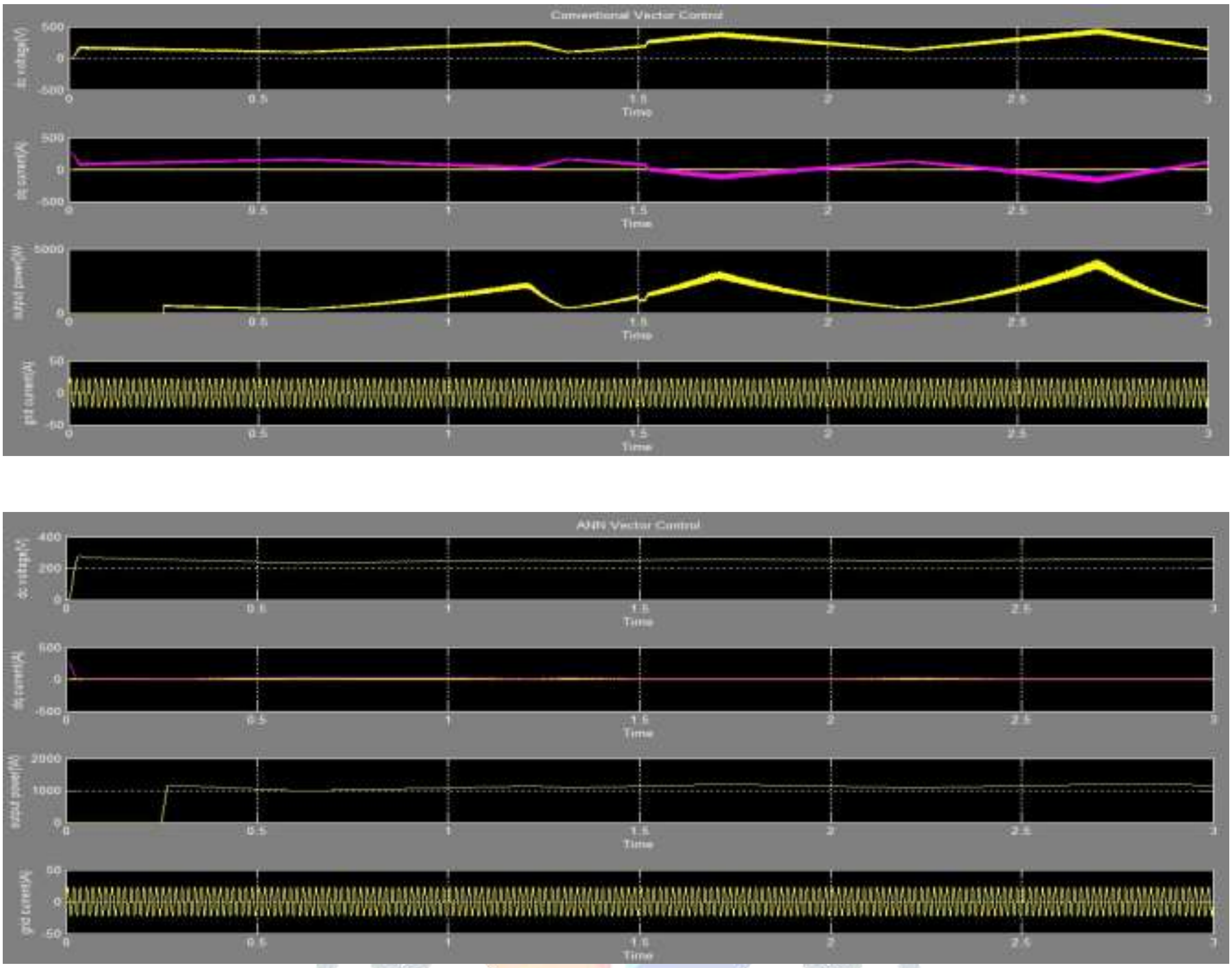

Fig.9 PR, VC, ANN control methods for variable irradiation:

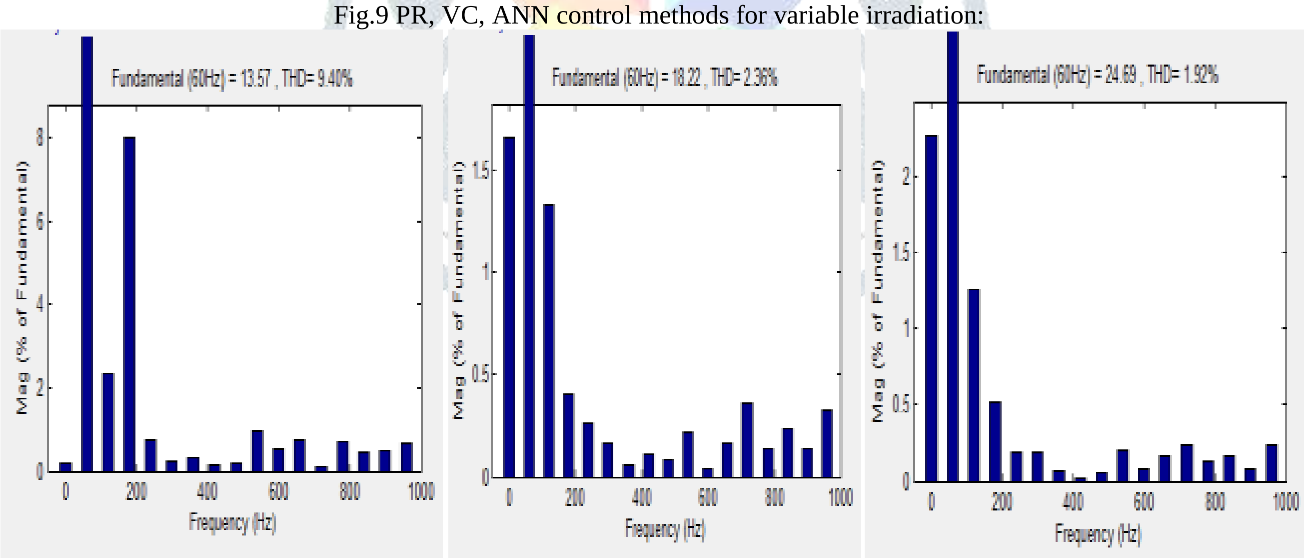

PR VC ANN

Fig.10 THD analysis for variable irradiation

The MPPT performance is slightly affected. The PCC current is more severely distorted, especially for the PR controlled PV system. The study demonstrates that the ANN controlled PV system has a strong adaptive capability under uncertain conditions although no further tuning is involved after the ANN is trained.

CONCLUSION:

This paper proposes a single-phase, residential solar PV system based on artificial neural networks and adaptive dynamic programming for MPPT control and grid integration of a solar photovoltaic array through an LCL-filter based inverter. The proposed artificial neural network controller implements the optimal control based on the approximate dynamic programming. The simulation results demonstrate that the solar PV system using the ADP-based artificial neural network controller has more improved performance than that using the proportional resonant or conventional standard vector control techniques, such as no requirement for damping resistance, more reliable and efficient extraction of solar power, more stable DC-link voltage, and more reliable integration with the utility grid. Using the

ADP-based neural network control technique, the harmonics are significantly reduced and the system shows much stronger adaptive ability under uncertain conditions, which would greatly benefit the integration of small-scale residential solar photovoltaic systems into the grid.

REFERENCES:

1 Renewable Energy World Editors. (2014, Nov. 12). Residential Solar Energy Storage Market Could Approach 1 GW by 2018. Available: http://www.renewableenergyworld.com.

2 R. A. Mastromauro, M. Liserre and A. D. Aquila, "Control Issues in Single-Stage Photovoltaic Systems: MPPT, Current and Voltage Control", *IEEE Trans. Ind. Informatics*, vol. 8, no. 2, pp. 241-254, May 2012.

3 E. Lorenzo, G. Araujo, A. Cuevas, M. Egido, J. Miñano and R. Zilles, *Solar Electricity: Engineering of Photovoltaic Systems*, Progensa, Sevilla, Spain, 1994.

4 J. M. Carrasco, L. G. Franquelo, J. T. Bialasiewicz, E. Galván, R. C. P.Guisado, M. Á. M. Prats, J. I. León, and N. Moreno-Alfonso, "Power-Electronic Systems for the Grid Integration of Renewable Energy Sources: A Survey", *IEEE Trans. Ind. Electron.*, vol. 53, no. 4, pp. 1002-1016, August 2006.

5 W. T. Franke, C. Kürtz and F. W. Fuchs, "Analysis of control strategies for a 3 phase 4 wire topology for transformer less solar inverters," in *Proc. IEEE Int. Symp. Ind. Electron.*, Bari, pp. 658-663, 2010.

6 B. Karanayil, V.G. Agelidis, and J. Pou, "Performance Evaluation of Three-Phase Grid-Connected Photovoltaic Inverters Using Electrolytic or Polypropylene Film Capacitors," *IEEE Trans. Sustain. Energy*, vol. 5, no. 4, pp. 1297-1306, Oct. 2014.

7 B. Bahrani, A. Rufer, S. Kenzelmann, and L. A. C. Lopes, "Vector control of single-phase voltage-source converters based on fictive-axis emulation," *IEEE Trans. Ind. Appl*., vol. 47, no. 2, pp. 831–840, Mar./Apr. 2011.

8 M. Castilla, J. Miret, J. Matas, L. G. Vicuña, and J. M. Guerrero, "Linear Current Control Scheme With Series Resonant Harmonic Compensator for Single-Phase Grid-Connected Photovoltaic Inverters," *IEEE Trans. Ind. Electron*., vol. 55, no. 7, pp. 2724–2733, July 2008.

9 A. Abrishamifar, A.A. Ahmad, and M. Mohamadian, "Fixed Switching Frequency Sliding Mode Control for Single-Phase Unipolar Inverters," *IEEE Trans. Power. Electron*., vol. 27, no. 5, pp. 2507–2514, May 2012.

10 M. El-Habrouk, M.K. Darwish, and P. Mehta, "Active power filters: A review," *IEEE Proc. Electric Power Applicat.*, vol.147, no 5, pp. 403– 413, Oct. 2000.

11 J. Lettl, J. Bauer, and L. Linhart, "Comparison of different filter types for grid connected inverter," in *Proc. Progress in Electromagnetics Research Symp.*, Marrakesh, Morocco, 2011, pp. 1426-1429.

12 J. Dannehl, C. Wessels, and F. W. Fuchs, "Limitations of voltage oriented PI current control of grid-connected PWM rectifiers with LCL filters," *IEEE Trans. Ind. Electron*., vol. 56, no. 2, pp. 380–388, Feb. 2009.

13 Z. Xin, P. C. Loh, X. Wang, F. Blaabjerg and Y. Tang, "Highly Accurate Derivatives for LCL-Filtered Grid Converter with Capacitor Voltage Active Damping," *IEEE Trans. Power. Electron.*, vol. 31, no. 5 pp. 3612-3625, May 2016.

14 H. Arritt, "Protection Practices for an Integrated Grid," in *Proc. IEEE Power & Energy Soc. General Meeting*, Denver CO, USA, 2015.

15 M. Veerachary, T. Senjyu and K. Uezato, "Neural-network-based maximum-power-point tracking of coupled-inductor interleaved-boost converter- supplied PV system using fuzzy controller," *IEEE Trans. Ind Electron.*, vol. 50, no. 4, pp. 749-758, Aug. 2003.

16 L. Wang and M. S. N. Thi, "Stability Enhancement of Large-Scale Integration of Wind, Solar, and Marine-Current Power Generation Fed to an SG-Based Power System Through an LCC-HVDC Link," *IEE Trans. Sustain. Energy*, vol. 5, no. 1, pp. 160-170, Jan. 2014.

17 F. J. Lin, K. C. Lu, T. H. Ke, B. H. Yang and Y. R. Chang, "Reactive Power Control of Three-Phase Grid-Connected PV System During Grid Faults Using Takagi–Sugeno–Kang Probabilistic Fuzzy Neural Network Control," *IEEE Trans. Ind. Electron*, vol. 62, no. 9, pp. 5516-5528, Sept. 2015.

18 F. J. Lin; K. C. Lu; B. H. Yang, "Recurrent Fuzzy Cerebellar Model Articulation Neural Network Based Power Control of Single-Stage Three-Phase Grid-Connected Photovoltaic System During Grid Faults," *IEEE Trans. Ind. Electron*., vol. 64, no. 2, pp. 1258-1268, Feb.2017.

19 N. Femia, D. Granozio, G. Petrone, G. Spaguuolo, and M. Vitelli, "Optimized One-Cycle Control in Photovoltaic Grid Connected Applications," *IEEE Trans. Aerosp. Electron. Syst.*, vol. 2, no. 3, pp.954-972, July 2006.

20 W. Wu, N. Pongratananukul, W. Qiu, K. Rustom, T. Kasparis and I. Batarseh, "DSP-based Multiple Peak Power Tracking for Expandable Power System," in *Proc. APEC, 2003*, pp. 525-530.

21 A. Kulkarni and V. John, "Mitigation of Lower Order Harmonics in a Grid-Connected Single-Phase PV Inverter," *IEEE Trans. Power Electron.*, vol. 28, no. 11, pp. 5024-5037, Nov. 2013

22 R. Teodorescu, F. Blaabjerg, M. Liserre, and P. C. Loh, "Proportional resonant controllers and filters for grid-connected voltage-source converters," in *IEE Proc. Elect. Power Appl.*, vol. 153, no. 5 pp. 750–762, Sep. 2006.

23 R. Zhang, M. Cardinal, P. Szczesny, and M. Dame, "A grid simulator with control of single-phase power converters in d-q rotating frame," in *Proc. IEEE 33rd Annu. Power Electron. Spec. Conf.*, Cairns, Queensland, Australia, 2002, pp. 1431–1436.

24 S. Li, T.A. Haskew, Y. Hong, and L. Xu, "Direct-Current Vector Control of Three-Phase Grid-Connected Rectifier-Inverter," *Electric Power Syst. Research*, vol. 81, no. 2, pp. 357-366, Feb. 2011.

25 S. H. Hwang, L. Liu, H. Li and J. M. Kim, "DC Offset Error Compensation for Synchronous Reference Frame PLL in Single-Phase Grid-Connected Converters," *IEEE Trans. Power Electron.*, vol. 27, no.8, pp. 3467-3471, Aug. 2012.

26 S. Haykin, "Neural Networks - A comprehensive foundation," Upper Saddle River, New Jersey: Prentice Hall, 1999.

27 F. Wang, H. Zhang, and D. Liu, "Adaptive dynamic programming: An introduction," *IEEE Comput. Intell. Mag.*, vol. 4, no. 2, pp. 39-47, May2009.